

This is the Accepted Manuscript version of an article accepted for publication in Smart Materials and Structures. IOP Publishing Ltd is not responsible for any errors or omissions in this version of the manuscript or any version derived from it. The Version of Record is available online at <https://doi.org/10.1088/0964-1726/25/8/085044>.

This manuscript version is made available under the CC-BY-NC-ND 4.0 license (<https://creativecommons.org/licenses/by-nc-nd/4.0/>)

# **Deformation monitoring of long GFRP bar soil nails using distributed optical fiber sensing technology**

by

Cheng-Yu Hong\* (Corresponding Author)

- a) Department of Civil Engineering, Shanghai University, Shanghai, China.
- b) State Key Laboratory of Earthquake Dynamics, Institute of Geology, China  
Earthquake Administration, Beijing 100029, China

Email: [cyhong@shu.edu.cn](mailto:cyhong@shu.edu.cn)

Jian-Hua Yin

Department of Civil and Environmental Engineering, The Hong Kong Polytechnic  
University, Hung Hom, Kowloon, Hong Kong, China

Tel: +852 2766 6065, Fax: +852 2334 6389, Email: [jian-hua.yin@polyu.edu.hk](mailto:jian-hua.yin@polyu.edu.hk)

Yi-Fan Zhang

Engineering Research Center of Technical Textiles, Ministry of Education, College  
of Textiles, Donghua University, China

Email: [zhangyifan@dhu.edu.cn](mailto:zhangyifan@dhu.edu.cn)

Manuscript submitted for possible publication as an article in the journal of *Smart  
Materials and Structures*

April 2016

## **Abstract**

This paper introduces a new measurement technology characterizing by the use of distributed optical fiber sensor for monitoring strain and temperature distribution of Glass Fiber Reinforced Polymer (GFRP) bar soil nails. Two lab tests including tensile and deflection tests were used to verify the performance of optical fiber sensors (OFS) for strain, elongation and deflection monitoring of GFRP bars. Two mathematical approaches including numerical integration method (NIM) and finite difference method (FDM) were used to predict deflection distributions at different bar locations. In verification tests, deflections predicted by FDM agree well with measured data, while NIM failed to predict deflections well. In field monitoring tests, two GFRP bar soil nails were installed with optical fiber sensors (OFS) and pure strain data were used for evaluating the performance of GFRP bar soil nails after installation. Brillouin Optical Time Domain Analysis (BOTDA) measurement unit was used to collect temperature and strain data from OFS. Measured axial elongations of soil nails were validated with the data predicted by a theoretical model. Monitoring data also show that both accumulative elongations and deflections of soil nails show continuous but limited rise as time elapses in field. The predicted deflections of FDM are almost half of the predictions using NIM. This discrepancy is mainly due to the linear assumption of deformed soil nail element using NIM, and sensor error may also accumulate from soil nail tip to head, affecting the final obtained deflection values.

Keywords: optical fiber sensor, GFRP bar soil nails, BOTDA, numerical integration method (NIM), finite difference method (FDM).

## **1 Introduction**

Optical fiber sensors (OFS) have been popular among geotechnical research communities in recent years for continuous strain and temperature distribution monitoring. Main advantages of OFS include small size, light weight, waterproofing, corrosion resistance, long durability, immune to electromagnetic interference (EMI), quick and simple installation methods, and wavelength multiplexing<sup>1-5</sup>. Brillouin Optical Time Domain Analysis (BOTDA) (or a similar technology Brillouin Optical Time Domain Reflectometry, BOTDR) based sensing technology is a promising method for distributed strain measurement of various geotechnical structures, such as piles<sup>6-8</sup>, soil nails<sup>9</sup>, slopes<sup>10</sup>, foundations<sup>7</sup>. Long soil nails are mostly adopted for the reinforcement of important geotechnical engineering structures such as high slopes, deep foundations and excavations. Performance monitoring of these soil nails is critical as they directly imply possible failure mode, as well as orientations of potential sliding surface of the whole reinforced projects. Long soil nails are difficult to monitor due to the long soil nail length where sensors have to be installed, as well as the harsh working environment which may possibly damage all sensors when placing soil nail bars into drill holes.

Past investigations using different sensing technologies such as traditional strain gauges, fiber Bragg grating (FBG) sensors have been reported in different literatures for performance assessment of piles or soil nails<sup>11-13</sup>. A typical limitation of these sensors is that they are “point sensors” or quasi-distributed sensors, and these sensors

failed to reflect the strain or temperature distribution in continuous space. Even for FBG which can be well multiplexed to form a sensing array, there are still very large space between adjacent sensors where the related strain or temperature data cannot be obtained. Fully distributed sensors such as BOTDA overcomes this typical limitation and can be used to replace thousands of “point sensors” over very long distance due to its fully distributed measurement feature. Currently there are limited investigations regarding the monitoring assessment of field soil nails using BOTDA sensing technology, though a number of other monitoring investigations have been conducted, such as the deformation measurement of tunnels, cuttings, and piles<sup>14-19</sup>; shape identification of composite materials using high resolution BOTDA technique<sup>7, 16</sup>, and landslide localization and prediction<sup>19</sup>.

Typical finding by Mohamad et al. (2007) and Mohamad et al. (2011)<sup>9, 20</sup> indicate that BOTDA based sensors are very powerful for performance assessment of piles or soil nails. The authors adopted numerical integration method for the calculation of pile deflections, which were then verified with measured data from inclinometers. Pile monitoring performed by Lu et al. (2012) indicate that BOTDA based sensors provide a comprehensive understanding of pile behavior under different vertical loading levels<sup>21</sup>. The occurred large compressive strains (around 1000  $\mu\epsilon$ ) of piles were successfully measured, and axial stress distribution, side friction and tip resistance of piles were well understood using OFS data. Huang et al. (2015) investigated the integrity displacement of a rod associated with interfacial damage evolution by using

BOTDA technology<sup>22</sup>. This BOTDA based build-in sensor is powerful and its performance has been verified in lab test. Hence, BOTDA technology offers an effective alternative for performance monitoring of large scale geotechnical structures.

This paper describes the application of using BOTDA technique for monitoring the deformation behavior of long Glass Fiber Reinforcement Polymer (GFRP) bar soil nails, which has already been considered as an alternative to replace traditional steel bars in different projects. Capability of BOTDA based OFS for field monitoring of long GFRP bar soil nails has been demonstrated by using basic calibration work, installation method of OFS, typical measurement data and the corresponding verification using an analytical model. This monitoring study offers a better understating of the behavior of long soil nails as reinforcements in slopes.

## **2 Measurement principle of BOTDA technique**

Fig.1 shows sensing principle of BOTDA based OFS used in present test. It is seen, two types of light including continuous wave light and pump pulse light are launched into two ends of a single OFS, when optical frequency difference between the continuous wave light and the pump pulse light matches the local Brillouin frequency of OFS, Brillouin scattering effect is stimulated and the light frequency shift generated by Brillouin scattering effect depends on the physical properties of OFS and hence can be used to evaluate the structural deformation due to temperature and strain

changes. Relationship between light frequency change  $\Delta\nu(\Delta T)$  and the related temperature change  $\Delta T$  when no strain change occurs is given by:

$$\Delta\nu(\Delta T) = C_T \Delta T \quad (1)$$

In practice, the OFS is normally subjected to both strain change  $\Delta\varepsilon$  and environmental temperature change  $\Delta T$ , hence the above equation can be updated as:

$$\Delta\nu(\Delta\varepsilon, \Delta T) = C_\varepsilon \Delta\varepsilon + C_T \Delta T \quad (2)$$

In the above two equations,  $C_T$  and  $C_\varepsilon$  are constant coefficients corresponding to temperature and strain change, respectively. Combing the above two equations, a new equation for the calculation of pure strain of OFS can be given by:

$$\Delta\varepsilon = [\Delta\nu(\Delta\varepsilon, \Delta T) - \Delta\nu(\Delta T)] / C_\varepsilon \quad (3)$$

Eq.(3) can be used to compute the pure strain change of OFS and hence the thermal effect on expansion and contraction of OFS structure can be eliminated. In present paper, two coefficient values are  $C_T = 0.001\text{GHz}/^\circ\text{C}$ ,  $C_\varepsilon = 0.5055\text{GHz}/\%$ <sup>23</sup>.

### **3 Verification tests for elongation and deflection measurement of GFRP bars**

#### *3.1 Strain and temperature sensors used in practical field*

Fig.2 shows schematic views of optical fiber strain sensors and temperature sensors used in present tests. The optical fiber strain sensor was bare OFS tightly packaged in Polyvinyl Chloride (PVC) jacket. Diameters of the external PVC jacket and inner bare optical fiber sensor are 1.8 mm and 125  $\mu\text{m}$ , respectively. The temperature sensor consists of two tight-buffered optical fibers for measuring the external temperature change, a stainless steel mono-coil tube for preventing the measurement of inner

deformation of optical fibers, and Kevlar as well as external PVC jacket for protecting the inner optical fiber cables. Diameters of the temperature sensor and inner tight-buffered optical fibers are 3.0 mm and 1.0 mm respectively. These packaged OFS were produced in Mainland China.

### 3.2 Elongation and deflection calculation using two mathematical methods

Elongation calculation of GFRP bars using BOTDA sensors can be simply achieved by integrating the length changes of all GFRP bar elements measured by OFS. Deflection calculation of GFRP bar element using distributed strain data is relatively complicated, and currently two typical methods were popular including numerical integration method (NIM) and finite difference method (FDM)<sup>24</sup>. NIM is a popular method for the calculation of deflection by considering the strain distributions measured by two symmetric optical fiber strain sensors mounted along GFRP bar surface. The corresponding curvature  $k$ , gradient  $a$ , and deflection  $u$  of GFRP bar can be obtained by <sup>20, 25</sup>:

$$k = \frac{1}{d}(\varepsilon_a - \varepsilon_b) \quad a = \int kdz + A \quad u = \int adz + B \quad (4)$$

where  $A$  and  $B$  are integration constants.  $\varepsilon_a$  and  $\varepsilon_b$  are the measured strain values along the two symmetric locations of the GFRP bar surface,  $d$  denotes the diameter of the GFRP bar.

FDM is a mathematical discretization method derived from Taylor's polynomial for solving differential equations. Distributed optical fiber sensors divide a deformed

beam into a number of small elements characterizing by measurement resolution of BOTDA unit. Length interval between adjacent beam elements is assumed to be  $h$ .

The first derivatives of  $f$  at distance values  $x$  and  $x-h$  are:

$$f'(x) = \frac{1}{h}[f(x+h) - f(x)] \quad (5)$$

$$f'(x-h) = \frac{1}{h}[f(x) - f(x-h)] \quad (6)$$

where  $f'(x)$  and  $f'(x-h)$  are deflection slopes with respect to the length of beam element. The second order derivative can be obtained by combing Eq.(5) and (6):

$$f'' = \frac{1}{h} \left\{ \frac{1}{h}[f(x+h) - f(x)] - \frac{1}{h}[f(x) - f(x-h)] \right\} = \frac{1}{h^2}[f(x+h) - 2f(x) + f(x-h)] \quad (7)$$

Figure 3 shows a schematic view of a typical beam deflection resulted from external loading. Assuming the beam deformation is small and  $Rd\theta = \Delta l \sim dx$ . Deflection gradient  $k = 1/R \sim d\theta/dx$ , rotation angle  $\theta \sim df/dx$ . Therefore, we have  $k \sim d^2 f / dx^2 = f''$ . The beam gradient can be given in terms of beam moment  $M$  and stiffness  $EI$ :

$$k = \frac{M}{EI} = f'' \quad (8)$$

Strain difference of two opposite directions of beam surface measured by OFS can also be written as:

$$\frac{\varepsilon_{ai} - \varepsilon_{bi}}{2} = \frac{M D}{EI 2} \quad (9)$$

where  $D$ ,  $E$  and  $I$  are thickness, elastic modulus and moment of inertia of the beam, respectively.  $\varepsilon_{ai}$  and  $\varepsilon_{bi}$  are the occurred strain at the upper and lower beam surface, respectively (as shown in Figure 3). Combing Eqs (7), (8) and (9) yields:

$$\frac{1}{h^2}[f(x+2h) - 2f(x+h) + f(x)] = \frac{\varepsilon_{ai} - \varepsilon_{bi}}{D} \quad (10)$$

Given the boundary conditions and measured strain distributions ( $\varepsilon_{ai}, \varepsilon_{bi}$ ) from OFS, beam deflections where mounted with strain sensors can be computed by Eq.(10). In present test, both NIM and FDM methods were used for the calculation of the deflection of GFRP bar soil nails in field.

### 3.3 Calibration tests and data comparison

Two laboratory tests including tensile and deflection tests were carried out to examine the performance of OFS for monitoring elongation and deflection of GFRP bar soil nails. Tensile test was carried out on a GFRP bar which was 40 mm in diameter and 0.8 m in length. Packaged optical fiber strain sensors were pretensioned and mounted on bar surface by using two worm metal drive clamps. The initial tensile strains of OFS mounted at two surface locations were between 3000 and 4000  $\mu\varepsilon$ . Tensile test was carried out by applying step by step load at one end of the GFRP bar and the other end was fixed. Load increment was 15 kN and a final 75 kN was approached after 5 loading steps. To verify the measured strain data of OFS, two strain gauges were mounted on the GFRP bar surface at the locations where mounted with OFS. Fig.4 (a) shows the relationships between measured frequency of OFS against optical fiber sensor distance. The OFS distance where with significant frequency increment (from around 3.8 m to 4.5 m and 8.5 m to 9.3 m) indicates the pretensioned locations of OFS. It is clear that the measured frequency increases uniformly as the tensile load increases from 15 kN to 75 kN. Frequency data change can be used to calculate the

occurred strains of the GFRP bar using Eq. (3) and temperature change is ignored as the tensile test was finished very soon (within one hour). Fig.4 (b) shows the comparison of measured tensile strain from strain gauges and OFS against applied load. Sensor 1# and Sensor 2# are two OFS sensors mounted at two symmetric locations in cross section of the GFRP bar surface. Average strain of OFS was compared with the average strain data of strain gauges and the two series of data agree fairly well as shown in Fig.4. Both of the two series of data increase linearly with the increase of applied load. The maximum strain obtained by strain gauge was around  $950 \mu\epsilon$ , but these strain gauges were damaged after tensile strain exceeds around  $1000 \mu\epsilon$ .

Deflection test was carried out by applying bending moment on a simply supported GFRP bar. Fig.5 shows a schematic view of the deflection test setup. OFS were mounted on both upper and lower surface of the GFRP bar and four linear variable displacement transducers (LVDT) were used to measure the occurred bar deflection at four locations. These four LVDTs divide the whole GFRP bar length between two supports into three equal lengths. A total of four OFS sections were mounted at upper and lower surface of GFRP bar and each section length was 2.4 m. Around  $5000 \mu\epsilon$  initial tensile strain was applied on OFS in order to measure the occurred compressive deformation. Similar to the tensile test, load was also applied step by step with a load increment of 9.8 N for each loading step, and five loading steps were finally conducted. Measured frequency variation against optical fiber sensor distance is

shown in Fig.6 (a). It is seen, the measured frequencies show substantial rise at four bar locations mounted with OFS. Each of these four OFS sections measures the same occurred strain. OFS as marked in this figure can be used to calculate beam deflections using NIM in Eq. (4) and FDM in Eq. (10). The measured and calculated deflections of different GFRP bar locations are compared in Fig.6 (b). It is clear that the measured deflections measured by LVDT agree fairly well with the predicted data of OFS using FDM. While NIM underestimates the occurred deflections significantly at some bar locations (distance values 1.2 m and 2.8 m). Fig.6 (c) shows the measured and predicted deflections at distance 1.6 m against loading values. All deflections increase linearly with the applied load. The predicted and measured deflections using FDM and LVDT agree fairly with each other, while the predicted deflection data using NIM are substantially lower than the true deflections, though a perfect linear relationship against loading level is obtained. This discrepancy is primarily due to the assumed linear assumption of bar element subjected to loading in calculation. It is noted that the boundary condition of the current deflection test is simply supported. Other boundary conditions can be considered if time and project budget are allowed to verify the performance of OFS for predicting the GFRP bar deflection.

#### **4 Installation of OFS in field and measurement data interpretation**

##### *4.1 Installation of OFS in the field*

GFRP bars maybe used as an alternative anchor tendon to replace traditional steel bars due to the advantages of excellent corrosion, high tensile strength, and light weight.

These characteristics make GFRP bars very convenient for transportation, installation and monitoring. In present field monitoring study, optical fiber sensors were mounted on the GFRP bar surface using the same method as introduced in tensile calibration test (Section 3.3). Figs.7 (a) to (e) show the installation of optical fiber strain and temperature sensors on GFRP bars in field. Fig.7 (a) shows the pretensioned OFS on the bar surface and fixed by worm metal driven clamps, and the GFRP bar installed with sensors is shown in Fig.7 (b). Fig.7 (c) shows the installation process of a GFRP bar into a drill hole in field. Figs.7 (d) and (e) show the strain and temperature sensors, as well as the sensor cables extending outside a drill hole, respectively.

#### *4.2 Strain and temperature data measured by OFS*

Fig. 8 shows the measured frequency distribution against optical fiber sensor distance at different measurement dates and sensor data were collected weekly. Initial readings were taken about one month after grouting. Soil nail head and tip locations are also marked in this figure. It is clear that the frequency distribution of optical fiber sensor is symmetric with respect to the GFRP soil nail tip. This is because the OFS used in present study formed a loop configuration measuring the strain distribution of the same GFRP bar but opposite surface. It is also seen that the measured frequency distribution shows obvious variations against OFS distance due to the non-uniform prestressed strain of OFS applied during installation process.

Fig.9 shows the frequency variations against optical fiber temperature sensor distance within one month (from one week to five weeks). Soil nail heads and tips are all marked in this figure. Similar to the previous symmetric frequency distribution of strain sensors, the temperature sensors inside the drill hole shows substantial change, while the sensors extended outside this drill hole (as marked in Fig.9) show relatively more obvious temperature change compared with sensor data inside drill hole. This observation indicates that the temperature change outside drill hole is relatively more obvious than that inside drill hole. The occurred temperature change will be used to calculate the pure strain change.

#### *4.3 Elongation and deflection of GFRP bar soil nails in the field*

Elongation can be calculated by integrating the element deformation characterized by average strain data of OFS mounted on GFRP bar surface. Figs.10 (a) and (b) show the occurred average strain against distance from heads of two GFRP bar soil nails E-A1 and E-A2. It is clear in the two figures that the mobilized strain values are mostly positive and increase from GFRP bar soil nail tip to head, indicating that soil nails were mainly subjected in tension. Tension strains (positive strain value) are relatively large in both middle regions (from 5 to 15 m for E-A1, and from 7 to 15 m for E-A2) and locations close to nail head (from 0 to 4 m for E-A1, from 0 to 5 m for E-A2). These average strain data can be used to obtain the occurred elongation of GFRP bar soil nails. Figs.11 (a) and (b) show the accumulative axial elongation of the two GFRP bar soil nails against distance from soil nail head in field. It is shown that,

elongations of the two soil nails show continuous increase as the distance from soil nail head decreases at different monitoring weeks. Accumulative elongations of both GFRP bar soil nails increase as time elapses for the two monitored soil nails. Maximum accumulative elongations of the two soil nails are quite limited, approaching around 0.4 mm in five weeks after initial readings of OFS was taken.

Deflection calculation of the two monitored GFRP bar soil nails can be achieved using NIM in Eq. (4) and FDM in Eq. (10). It is noted that the boundary condition of soil nail tip is assumed to be fixed, that is, neither initial rotation nor initial displacement of the soil nail tip was taken into account in calculation. Figs.12 (a) and (b) show the occurred deflection of GFRP bar soil nails E-A1 and E-A2 using NIM and FDM. Deflections of the two GFRP bars increase from soil nail tip to soil nail head at different measurement weeks. Deflections develop gradually as time elapses, and the maximum deflections which normally occur at soil nail heads approach around 55 mm (NIM) and 28 mm (FDM) for E-A1, and 52 mm (NIM) and 25 mm (FDM) for E-A2, respectively. It is noted the deflection of soil nail head indicates the related lateral movement with respect to nail tip, not the absolute soil nail head movement on slope surface. This occurred GFRP deflections are possibly caused by creep ground movement, and these deflection magnitudes are quite limited and can be ignored in comparison with lengths of these soil nails (more than 30 m). It is also clear in this figure that the predicted deflections by NIM are substantially larger than that of FDM. The main reason maybe attributed to the linear assumption of deformed

GFRP bar element in calculation, leading to accumulative errors when deformation is relatively large. Maximum deflections of the two GFRP bar soil nails computed using NIM and FDM are summarized in Table 1. It is also seen that the all the predicted maximum deflections of GFRP bars by NIM are almost twice of the FDM, indicating that NIM overestimates true deflections significantly. In next section, a case study is presented to evaluate the effectiveness of NIM for deflection calculation.

#### *4.4 A case study of deflection calculation of GFRP bar soil nails using NIM and FDM*

To verify the effectiveness of using NIM and FDM for deflection calculation of soil nails, a case study is presented regarding an ideal soil nail subjected to lateral pressure. Diameter and length of a soil nail bar are assumed to be 1 m and 10 m, respectively. Elastic modulus of soil nail is assumed to be 30 GPa. Assumed later pressures per meter length are 0.5 kN/m, 1 kN/m and 2 kN/m, and the soil nail tip is assumed to be fixed end. Fig.13 shows comparison of theoretical and calculated deflections of soil nails subjected to lateral pressure using the above two methods. TD refers to theoretical deflection in this figure. It is obvious the NIM overestimates the occurred deflections significantly (about 18% in average) at all different loading levels, while all predictions of FDM agree fairly well with theoretical values. Therefore, correction coefficients should be used to modify the deflections computed from NIM, in order to have a better prediction of the true deflections.

#### 4.5 Comparison of elongation of GFRP bar soil nails with predictions of theoretical models

Soil nails as slender bars were normally subjected to tension under service state in slopes, and excavations. Pullout effect of soil nails maybe motivated by ground creep movement, which further generates pullout reaction force at soil nail head with concrete girder over slope surface. Some typical analytical models have been proposed in past few decades to investigate the pullout performance of cement grouted soil nails. Assuming a soil nail is subjected to pullout force at soil nail head (for example, reaction force occurred at soil nail head), the pullout displacement (accumulative elongation) at different distance with respect to soil nail tip can be obtained considering elasticity of soil nails<sup>26, 27</sup>:

$$u(x) = -\frac{P}{\pi k D} \frac{\lambda \cosh(\lambda x)}{\lambda \sinh(\lambda x)} \quad (11)$$

where  $u(x)$ ,  $P$ ,  $k$ , and  $D$  are accumulative elongation at distance  $x$  from nail tip, pullout force, stiffness factor, and diameter of soil nail.  $\lambda = \sqrt{\frac{k\pi D}{E_e A}}$  is scaling factor.

$E$  and  $A$  are elastic modulus and cross sectional area of the GFRP bar soil nail. in this study, reaction force values generated at soil nail heads are assumed to be 10, 12, 14 kN and 9, 11, 13 kN, respectively for E-A1 and E-A2 at one week, three weeks, and five weeks after initial reading were taken. Hence the accumulative elongation of a soil nail at different axial distance under pullout force  $P$  can be obtained by using Eq. (11). Figs.13 (a) and (b) show comparisons between calculated accumulative axial elongation using equation Eq. (11) and the measured elongation in present test. All

parameter values adopted in this analytical model are summarized in Table 2, where  $A$ ,  $A_c$ , and  $A_g$  are cross sectional areas of whole soil nail, concrete and GFRP bar, respectively.  $E_c$ ,  $E_g$ , and  $E_e$  are elastic moduli of concrete, GFRP bar, and effective elastic modulus, respectively. It is clear that the predicted elongation values mostly agree well with the measured data in present tests, indicating that the monitoring data are reliable and can be successfully predicted using analytical models taking into account the soil nail property parameters in field.

## 5 Conclusions

This paper presents a typical study using fully-distributed optical fiber sensors for monitoring the performance of GFRP bar soil nails in a real field. Calibration work, basic installation procedures, typical monitoring data and a comprehensive analysis are presented to better understand the mechanical behavior of GFRP bar soil nails. The followings are typical findings and conclusions of this monitoring study:

- a) Calibration tests in this study indicate that the designed optical fiber sensors, installation scheme of OFS, calculation method for computation of elongations and deflections of GFRP bar soil nails are reliable.
- b) GFRP bar soil nails were subjected slightly tension effect and axial elongations show continuous rise as time elapses. The occurred accumulative axial elongations of soil nails were verified with predictions of a theoretical model in literature. Therefore, the full distributed optical fiber sensors offer an ideal and reliable method to better understand the mechanical performance of soil nails in

field, as traditional sensors are normally point sensors and difficult to measure strain distributions in continuous space.

- c) Two mathematical methods including finite difference method and numerical integration method were used to predict deflections of GFRP bar soil nails in field after cement grout in drill holes has hardened. (NIM). Predicted deflections using FDM agree fairly well with measured data, but deflections calculated using NIM present substantial discrepancies in both calibration test and field calculations. The occurrence of this discrepancy maybe attributed to the linear assumption of soil nail element especially when relatively large deformation occurred. Therefore, FDM is suggested to be used for deflection prediction of long soil nails in future.

The present work only considered the monitoring of GFRP bar soil nails as a typical investigation. Some other conventional sensors such as strain gauges were not adopted for comparison with measured strain data due to the limited budget and time. Other fully-distributed sensing technologies, such as Brillouin Optical Time Domain Reflectometry (BOTDR) or Low Coherence Interferometry, (LCI) are suggested to verify the present sensor performance.

### **Acknowledgement**

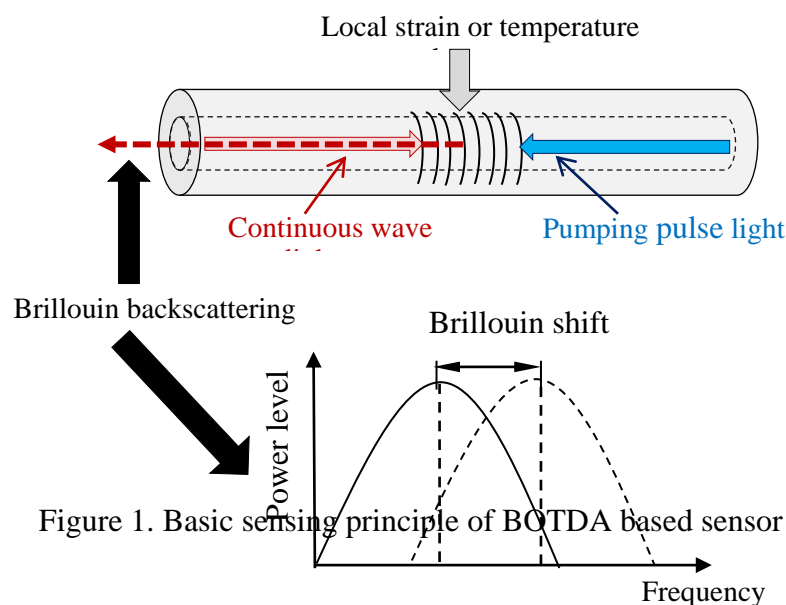
The authors would like to thank the kind support from Dr. Xu Dong-Sheng and Dr. Pei Hua-Fu during the installation of optical fiber sensors and monitoring. This work was also supported by the State Key Laboratory of Earthquake Dynamics, Institute of

Geology, China Earthquake Administration (Project No: LED2013B01) and the Fundamental Research Funds for the Central Universities (Project No: 15D110153 and 15D110136).

## References

1. W. W. Morey, G. Meltz and W. H. Glenn 1990 Fiber optic Bragg grating sensors. *Proc., OE/FIBERS'89*, International Society for Optics and Photonics, 98-107.
2. J. H. Yin, H. H. Zhu, K. W. Fung, W. Jin, L. M. Mak and K. Kuo 2008 Innovative optical fiber sensors for monitoring displacement of geotechnical structures. *Proc., Proceedings of the HKIE Geotechnical Division 28th Annual Seminar, Hong Kong*, 287-294.
3. P. Ferdinand, S. Magne, V. Dewynter-Marty, C. Martinez, S. Rougeault and M. Bugaud 1997 Applications of Bragg grating sensors in Europe. *Proc., Optical Fiber Sensors*, Optical Society of America, OTuB1.
4. M. Majumder, T. K. Gangopadhyay, A. K. Chakraborty, K. Dasgupta and D. K. Bhattacharya 2008 Fibre Bragg gratings in structural health monitoring—Present status and applications *Sensors and Actuators A: Physical* **147** (1) 150-164.
5. D. Inaudi, École Polytechnique, 1997.
6. P. Bourne-Webb, B. Amatya, K. Soga, T. Amis, C. Davidson and P. Payne 2009 Energy pile test at Lambeth College, London: geotechnical and thermodynamic aspects of pile response to heat cycles *Geotechnique* **59** (3) 237-248.
7. A. Klar, P. J. Bennett, K. Soga, R. J. Mair, P. Tester, R. Fernie, H. D. St John and G. Torp-Peterson 2006 Distributed strain measurement for pile foundations *Proceedings of the ICE-Geotechnical Engineering* **159** (3) 135-144.
8. H. Mohamad, K. Soga, A. Pellew and P. J. Bennett 2011 Performance monitoring of a secant-piled wall using distributed fiber optic strain sensing *J Geotech Geoenviron* **137** (12) 1236-1243.
9. B. Amatya, K. Soga, P. Bennett, T. Uchimura, P. Ball and R. Lung 2008 Installation of optical fibre strain sensors on soil nails used for stabilising a steep highway cut slope. *Proc., Advances in Transportation Geotechnics: Proceedings of the International Conference held in Nottingham, UK, 25-27 August 2008*, CRC Press, 277.
10. Y. J. Sun, D. Zhang, B. Shi, H. J. Tong, G. Q. Wei and X. Wang 2014 Distributed acquisition, characterization and process analysis of multi-field information in slopes *Engineering Geology* **182** 49-62.
11. H. F. Pei, C. Li, H. H. Zhu and Y. J. Wang 2013 Slope Stability Analysis Based on Measured Strains along Soil Nails Using FBG Sensing Technology *Mathematical Problems in Engineering* **2013**
12. C. Y. Hong, J. H. Yin, H. F. Pei and P. Lin 2013 Performance Monitoring of Cement Grouted Soil Nails in Cut Slopes Using Fiber Bragg Grating Sensors. *The 6th International Conference on Structural Health Monitoring of Intelligent Infrastructure, Hong Kong, China*
13. H. H. Zhu, J. H. Yin, A. T. Yeung and W. Jin 2010 Field pullout testing and performance evaluation of GFRP soil nails *J Geotech Geoenviron* **137** (7) 633-641.
14. C. Y. Hong, J. H. Yin, W. Jin, C. Wang, W. H. Zhou and H. H. Zhu 2010 Comparative Study on the Elongation Measurement of a Soil Nail Using Optical Lower Coherence Interferometry Method and FBG Method *Adv Struct Eng* **13** (2) 309-319.
15. J. F. Davalos, Y. Chen and I. Ray 2008 Effect of FRP bar degradation on interface bond with high strength concrete *Cement Concrete Comp* **30** (8) 722-730.

16. C. Li, Y.-G. Zhao, H. Liu, Z. Wan, C. Zhang and N. Rong 2008 Monitoring second lining of tunnel with mounted fiber Bragg grating strain sensors *Automation in Construction* **17** (5) 641-644.
17. W. H. Zhou, J. H. Yin and C. Y. Hong 2011 Finite element modelling of pullout testing on a soil nail in a pullout box under different overburden and grouting pressures *Can Geotech J* **48** (4) 557-567.
18. C. Li, Y. G. Zhao, H. Liu, Z. Wan, J. C. Xu, X. P. Xu and Y. Chen 2009 Strain and back cavity of tunnel engineering surveyed by FBG strain sensors and geological radar *Journal of Intelligent Material Systems and Structures*
19. M. Iten, A. M. Puzrin and A. Schmid 2008 Landslide monitoring using a road-embedded optical fiber sensor - art. no. 693315 *P Soc Photo-Opt Ins* **6933** 93315-93315.
20. H. Mohamad, K. Soga, A. Pellew and P. J. Bennett 2011 Performance monitoring of a secant-piled wall using distributed fiber optic strain sensing *J Geotech Geoenviron* **137** 1236-1243.
21. Y. Lu, B. Shi, G. Wei, S.-E. Chen and D. Zhang 2012 Application of a distributed optical fiber sensing technique in monitoring the stress of precast piles *Smart Materials and Structures* **21** (11) 115011.
22. M. Huang, Z. Zhou, Y. Huang and J. Ou 2013 A distributed self-sensing FRP anchor rod with built-in optical fiber sensor *Measurement* **46** (4) 1363-1370.
23. U. M. D. S.-R. Fiber Optic Distributed Temperature and Strain Analyzer, Internet: [//www.omnisens.com](http://www.omnisens.com), (2008).
24. D. S. Xu, J. H. Yin, Z. Z. Cao, Y. L. Wang, H. H. Zhu and H. F. Pei 2013 A new flexible FBG sensing beam for measuring dynamic lateral displacements of soil in a shaking table test *Measurement* **46** (1) 200-209.
25. H. Mohamad, P. J. Bennett, K. Soga, A. Klar and A. Pellow 2007 Distributed optical fiber strain sensing in a secant piled wall. *Proc., Proceedings of the 7th International Symposium on Field Measurements in Geomechanics*, ASCE Geotechnical Special Publication (GSP), 81.
26. A. Misra, C.-H. Chen, R. Oberoi and A. Kleiber 2004 Simplified analysis method for micropile pullout behavior *J Geotech Geoenviron* **130** (10) 1024-1033.
27. C. Y. Hong, J. H. Yin, W. H. Zhou and H. F. Pei 2011 Analytical study on progressive pullout behavior of a soil nail *J Geotech Geoenviron* **138** (4) 500-507.



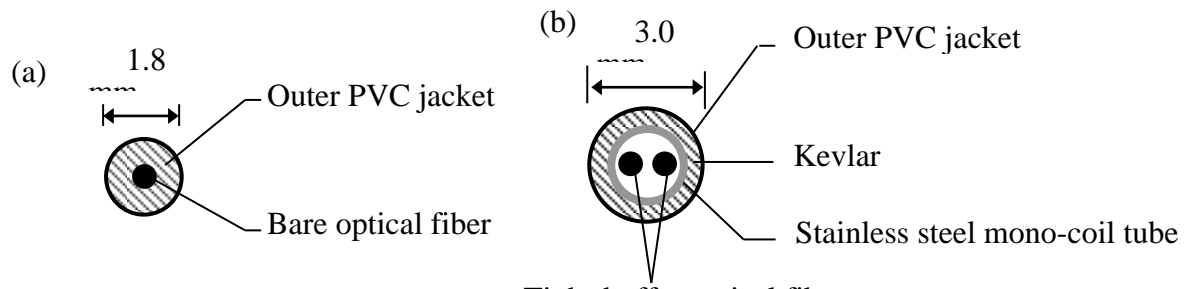
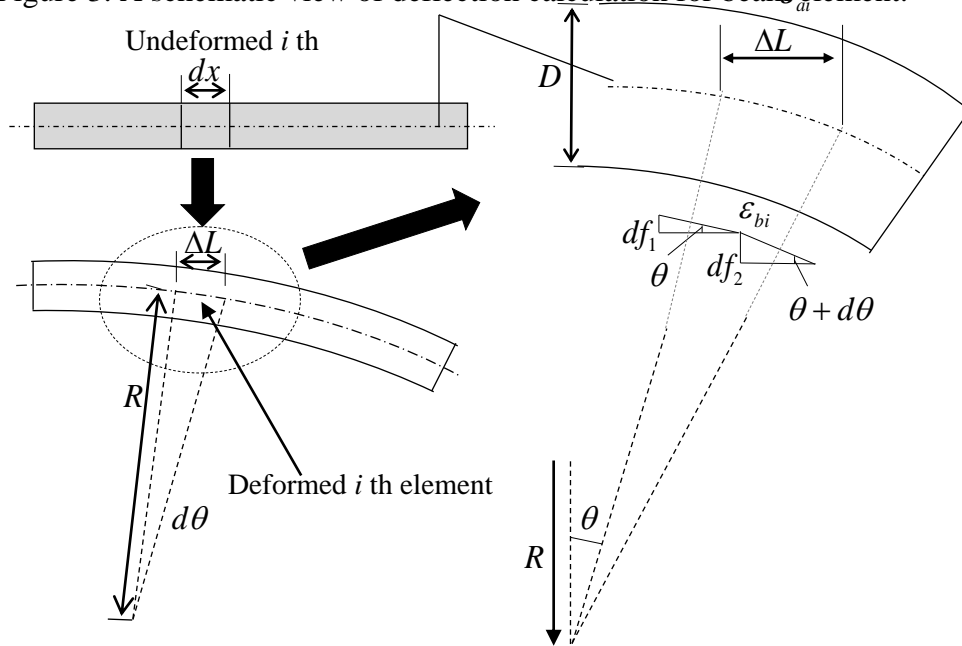
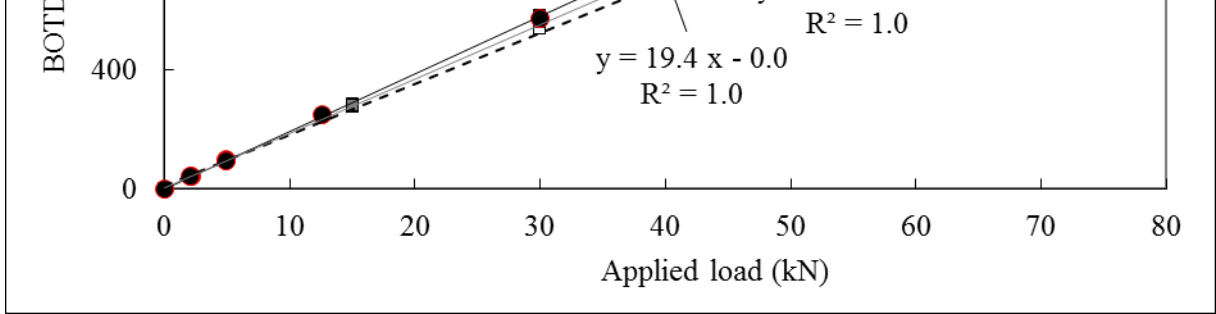


Figure 2. Schematic views of internal structures of (a) optical fiber strain sensor; and (b) optical fiber temperature sensor.

Figure 3. A schematic view of deflection calculation for beam element.

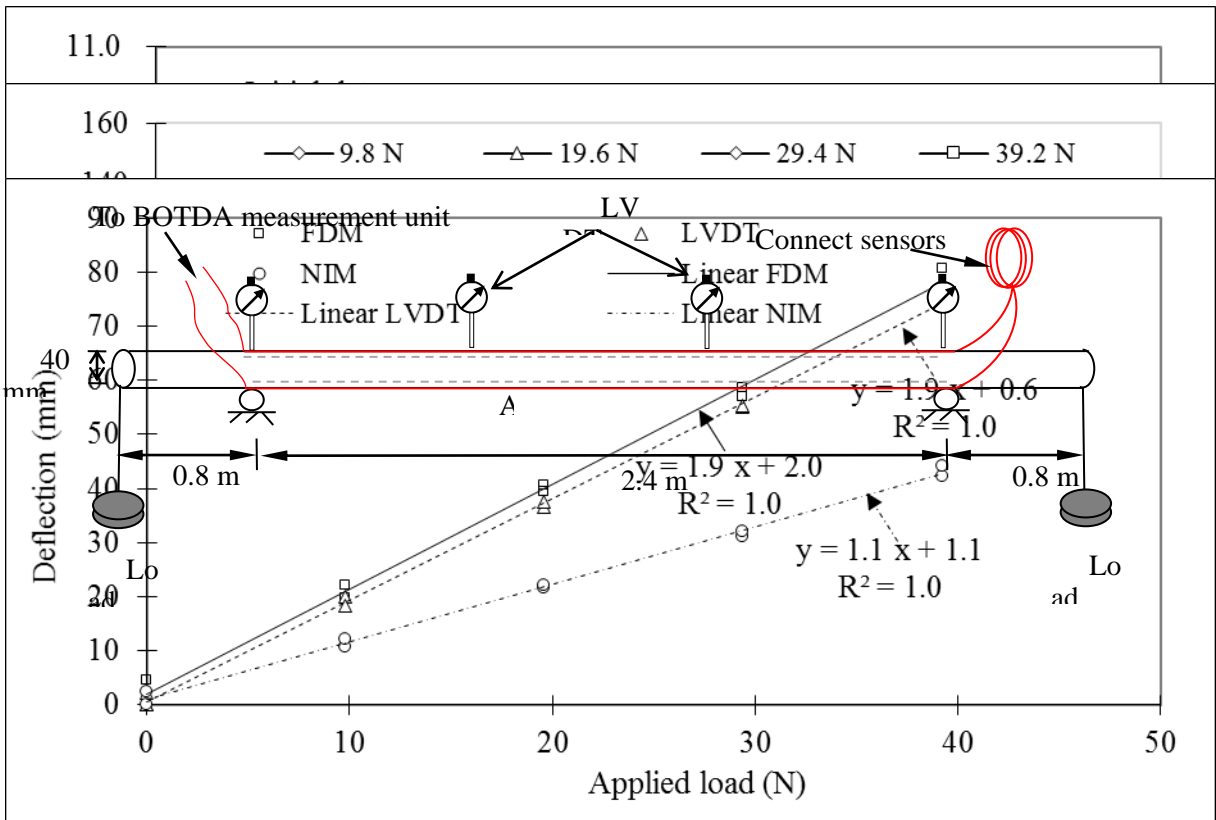


$d \theta_i$



(b)

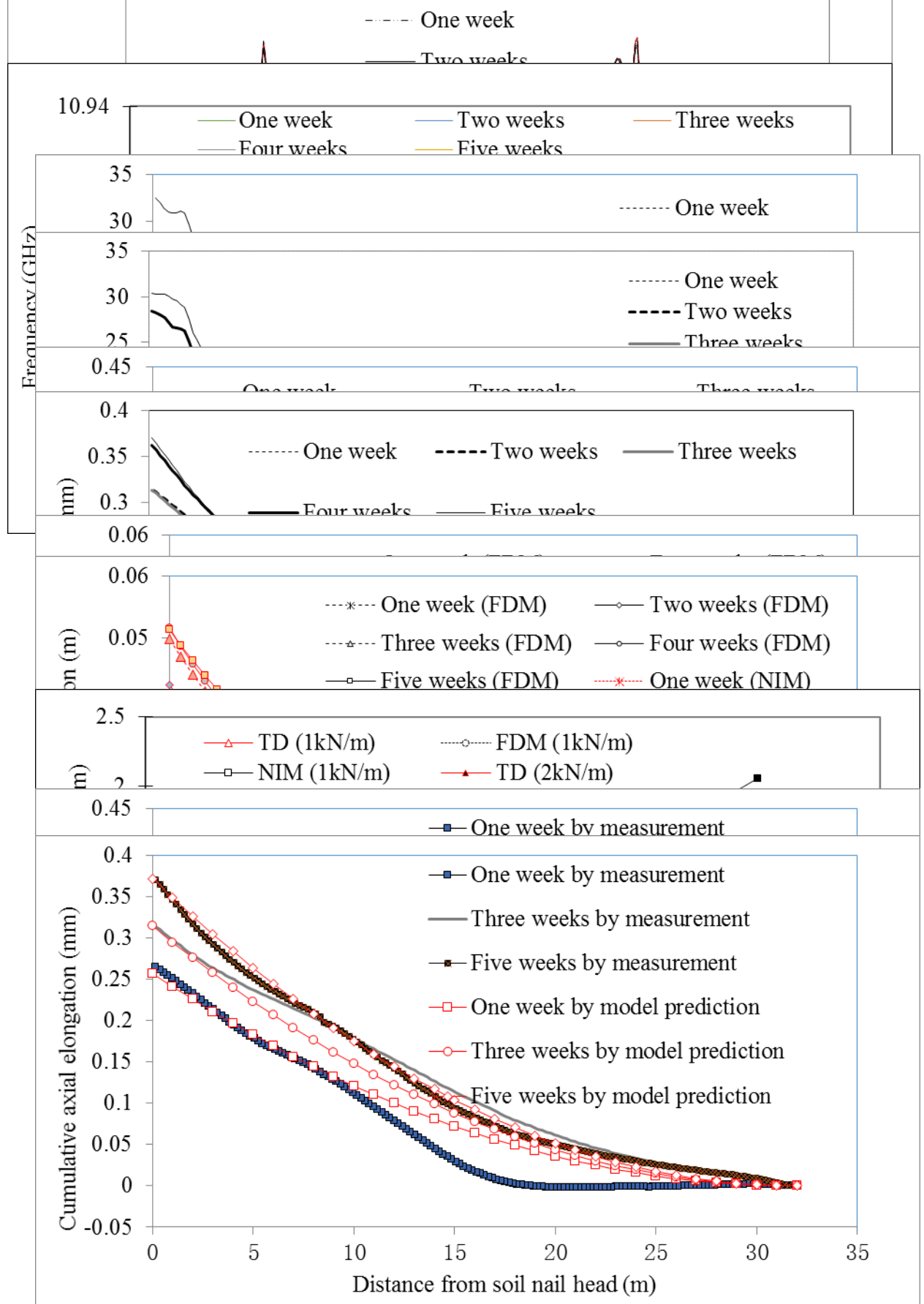
Figure 4. Measured frequency and strain data of optical fiber sensors - (a) relationships of frequency against optical fiber sensor distance; and (b) relationships of measured strain data against applied load in tension test for a GFRP bar.



(c)

Figure 6. Relationships of (a) measured frequency against optical fiber sensor distance, and (b) measured and calculated deflections of GFRP bars using NIM and FDM, and (c) calculated and measured deflections of Point A against applied load of the GFRP bar.





(b)

Figure 14. Comparison of cumulative axial elongation against distance from soil nail head at different measurement dates for soil nails (a) E-A1, and (b) E-A2.

Table 1. Maximum deflections of GFRP bar soil nail heads calculated by FDM and NIM methods.

| Method     | One week | Two weeks | Three weeks | Four weeks | Five weeks |
|------------|----------|-----------|-------------|------------|------------|
| NIM (E-A1) | 0.031    | 0.045     | 0.045       | 0.050      | 0.055      |
| FDM (E-A1) | 0.015    | 0.022     | 0.022       | 0.025      | 0.027      |
| NIM (E-A2) | 0.030    | 0.042     | 0.050       | 0.052      | 0.051      |
| FDM (E-A2) | 0.015    | 0.021     | 0.025       | 0.025      | 0.025      |

Table 2. Parameters adopted for the verification of cumulative axial elongation for GFRP bar soil nails.

| Parameter | $D$<br>(m) | $A$<br>(m <sup>2</sup> ) | $A_c$<br>(m <sup>2</sup> ) | $A_g$<br>(m <sup>2</sup> ) | $E_c$<br>(GPa) | $E_g$<br>(GPa) | $E_e$<br>(GPa) | $k$<br>(kPa) | $\lambda$<br>(m <sup>-0.5</sup> ) |
|-----------|------------|--------------------------|----------------------------|----------------------------|----------------|----------------|----------------|--------------|-----------------------------------|
| value     | 0.15       | 0.017671                 | 0.016415                   | 0.001257                   | 30             | 50             | 31.4           | 100          | 0.009212                          |